NANO LETTERS

2007
Vol. 7, No. 3
588−595

Resonant Excitation and Imaging of Nonequilibrium Exciton Spins in Single Core–Shell GaAs–AlGaAs Nanowires

Thang Ba Hoang,[†,‡] Lyubov V. Titova,[†] Jan M. Yarrison-Rice,[§] Howard E. Jackson,[†] Alexander O. Govorov,[||] Yong Kim,[⊥,#] Hannah J. Joyce,[#] H. Hoe Tan,[#] Chennupati Jagadish,[#] and Leigh M. Smith*[,†]

Department of Physics, University of Cincinnati, Cincinnati, Ohio 45221-0011, Department of Physics, Miami University, Oxford, Ohio 45056, Department of Physics and Astronomy, Ohio University, Athens, Ohio 45701, Department of Electronic Materials Engineering, Research School of Physical Sciences and Engineering, Australian National University, Canberra ACT 0200, Australia, and Department of Physics, College of Natural Science, Dong-A University, Hadan 840, Sahagu, Busan 604-714, Korea

Received October 10, 2006; Revised Manuscript Received December 12, 2006

ABSTRACT

Nonequilibrium spin distributions in single GaAs/AlGaAs core–shell nanowires are excited using resonant polarized excitation at 10 K. At all excitation energies, we observe strong photoluminescence polarization due to suppressed radiative recombination of excitons with dipoles aligned perpendicular to the nanowire. Excitation resonances are observed at 1- or 2-LO phonon energies above the exciton ground states. Using rate equation modeling, we show that, at the lowest energies, strongly nonequilibrium spin distributions are present and we estimate their spin relaxation rate.

Semiconductor nanowires have recently attracted considerable attention as the building blocks for nanoscale photonic devices such as lasers,[1,2] photodetectors,[3,4] and LEDs[5] as well as device interconnects.[6−8] The success of these devices depends upon the fact that semiconductor nanowires allow one to control the confinement of the electronic states through discontinuities of the semiconductor band gap and at the same time control the electromagnetic field through the discontinuities of the dielectric constants. Recent demonstrations of nanowire radial and axial heterostructures[9−11] open vast opportunities for engineering the bandstructure, strain, and dielectric properties of the nanowires. Indeed, such heterostructures have been used recently to create single photon emitters[12] and single electron transistors.[13] Despite these early successes, very little is known about the dynamics of the electronic states within the nanowire or the impact of the modified electromagnetic field on those dynamics.

In this letter, exciton dynamics derived from CW polarization-resolved photoluminescence excitation spectra obtained from single GaAs/AlGaAs core−shell nanowires at low temperatures using slit-confocal microscopy are presented.[14−17] The core in these nanowires is approximately 40 nm, so one expects only negligible quantum confinement for the electronic states. However, *both* the excitation and emission of excitons is strongly polarized along the nanowire because of the dielectric mismatch between the semiconductor nanowire and the surrounding air.[17,18] Here, we show that the suppression of the electromagnetic (photon) field in these nanowires results directly in a corresponding suppression of the radiative rate (increased radiative lifetime) for excitonic dipoles aligned perpendicularly to the nanowire. These excitons become essentially "dark." Most importantly, we show that the spin and relaxation dynamics can be studied through resonant excitation of excitons into well-defined spin states and polarization analysis of the emitted photoluminescence. Strong excitation resonances are observed due to efficient relaxation of excitons through the emission of LO phonons. Polarization measurements as a function of energy show directly that significant nonequilibrium distributions of excitons can be created through resonant excitation. A simple coupled rate-equation model is used to estimate an

* Corresponding author. E-mail: leigh.smith@uc.edu.
[†] Department of Physics, University of Cincinnati.
[‡] On leave from Institute of Materials Science, VAST, Hanoi, Vietnam.
[§] Department of Physics, Miami University.
[||] Department of Physics and Astronomy, Ohio University.
[⊥] Department of Physics, Dong-A University.
[#] Department of Electronic Materials Engineering, Australian National University.

10.1021/nl062383q CCC: $37.00
Published on Web 02/15/2007

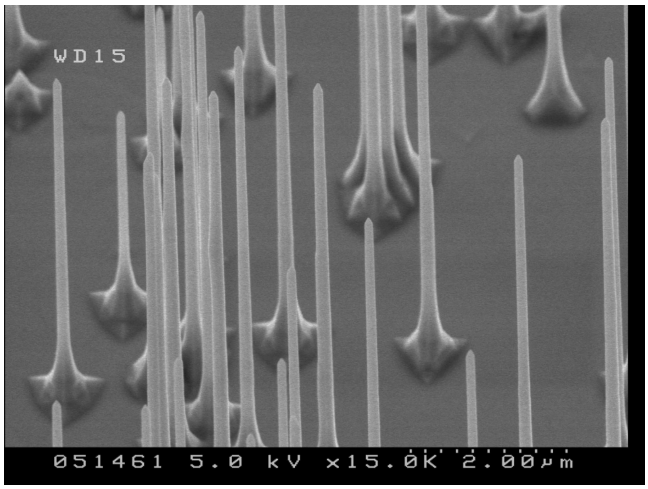

Figure 1. SEM micrograph of GaAs−AlGaAs nanowires on a GaAs substrate

upper bound to the spin-scattering rate for excitons confined to these nanowires.

GaAs/AlGaAs nanowire samples were fabricated by the VLS method.[19] Undoped GaAs (111)B substrates were functionalized by dipping in 0.1% poly-L-lysine (PLL) solution for 1 min. After rinsing and drying, 30 nm diameter Au nanoparticles were dispersed on the substrate surface. The substrate was annealed in situ at 600 °C under AsH_3 ambient in an MOCVD chamber for 10 min to desorb surface contaminants and form a eutectic alloy between the Au nanoparticle and Ga from the substrate. After cooling down to the growth temperature at 450 °C, trimethylgallium (TMG) source gases were switched on to initiate nanowire growth. The approximately 40 nm diameter GaAs nanowires were grown along the (111)*B* axis. After increasing the growth temperature to 650 °C, shell growth was initiated by switching off the TMG source and switching on trimethylgallium (TMG) and trimethylaluminum (TMA) sources simultaneously. The vapor aluminum composition was 0.26. Figure 1 shows a field-emission electron microscope (FESEM) image of the NWs grown at the same time as the nanowires studied here. The nanowires have a pronounced tapered shape, with average diameters of 80−160 nm and average lengths of 6−8 μm. Transmission electron micrographs of bare GaAs nanowires (not shown here) show similar degrees of tapering, but with average diameters of 40 to 60 nm.

To carry out single nanowire measurements, nanowires were removed from the growth substrate into solution and deposited onto a silicon substrate patterned with a crossing lattice of alignment marks. The substrate with the nanowires was placed in a variable temperature continuous flow helium optical cryostat. A CW Ti:sapphire laser, tunable from 705 to 808 nm, was used as the excitation source. The 10 mW laser beam was defocused to a 10 μm spot size in order to illuminate the entire nanowire of interest. At this excitation power and wavelength, fewer than 100 excitons are excited within the nanowire at any given time, ensuring that the excitons are essentially noninteracting. The PL emitted from a single nanowire was imaged using a 50×/0.5NA micro-

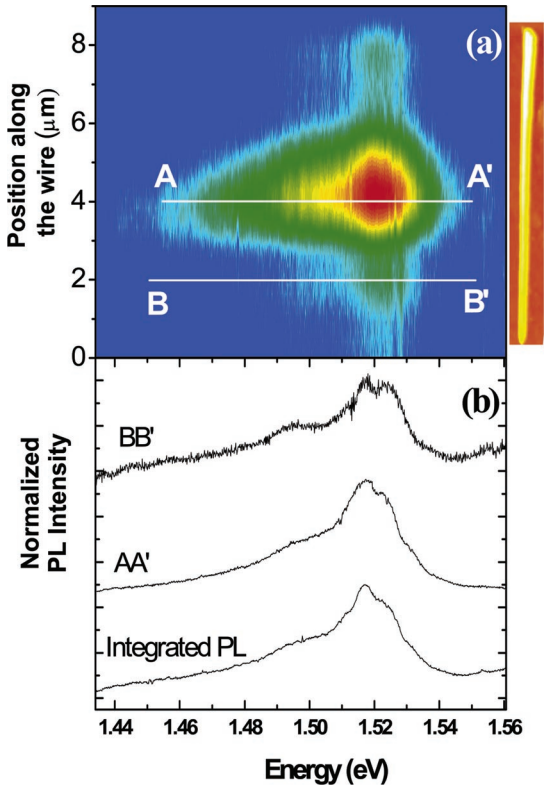

Figure 2. Photoluminescence imaging of wire 1 at 10 K: (a) 2D map of the wire 1 emission; on the right is an AFM micrograph of the wire; the wire is 7.4 μm long, with average diameter of 120 nm (b) PL spectra extracted from the 2D map at the positions specified by the lines in (a) and integrated PL spectrum from the entire nanowire.

scope objective. The orientation of the single nanowire was adjusted so as to align its 350× image along the entrance slit of the spectrometer. The collected PL was dispersed by a $^1/_4$ m focal length imaging spectrograph with a 1200 groove grating and detected by a 1024 × 124 pixel thermoelectrically cooled charge-coupled device (CCD) detector. This configuration allowed us to collect the spectral and spatial information simultaneously by recording two-dimensional (2D) PL maps. All the measurements were conducted at 10 K. The spatial resolution for this configuration is ∼1.5 μm. A detailed study of the optical characterization and the temperature dependence of the emission from these single core−shell GaAs−AlGaAs nanowires can be found elsewhere.[17] Here, we note only that the recombination lifetimes in these nanowires is <80 ps when measured using time-correlated single photon counting at low temperatures at the same excitation wavelength under similar conditions, and so exciton dynamics is dominated by nonradiative recombination.

Significant excitation-resolved data were studied in several nanowires; representative detailed results from two nanowires (referred to as wire 1 and wire 2) will be discussed here. A typical 2D PL map of wire 1 for 750 nm laser excitation is displayed in Figure 2a. In this image, the vertical axis corresponds to the spatial position along the nanowire, and the horizontal axis denotes the emission energy. An AFM

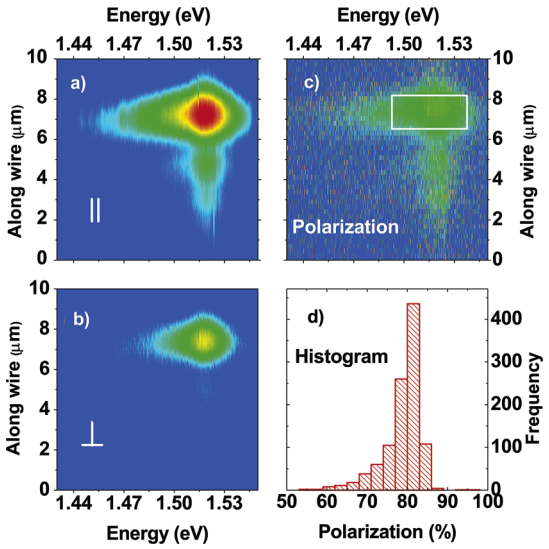

Figure 3. Polarization-resolved photoluminescence imaging of the wire 2 at 10 K: (a) 2D map of wire 2 emission polarized parallel to the wire; (b) 2D map of the wire 2 emission polarized perpendicular to the wire with identical intensity color mapping to map in (a); (c) 2D emission polarization map. Blue is less than 65%, green is 80%, red is 97%; (d) histogram of the polarization for a set of pixels defined by the box in (c)

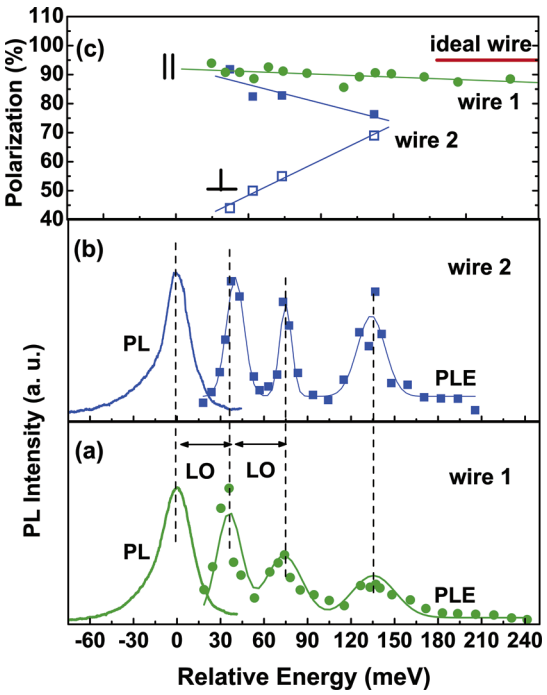

Figure 4. Photoluminescence excitation spectroscopy: (a) PL (solid line) and PLE (solid line with solid circles) for wire 1; (b) PL (solid line) and PLE (solid line with solid squares) for wire 2; solid lines are Gaussian fits to PLE spectra. (c) Degree of linear polarization of PL emission as a function of excitation laser energy for wire 1 (circles) and wire 2 (squares). For laser polarized parallel to wire 1 (solid circles) and wire 2 (solid squares), degree of emission polarization decreases with increasing laser energy. For laser polarized perpendicular to wire 2 (open squares), the degree of polarization increases with increasing laser energy.

image of wire 1 shown to the right of the PL image indicates that the wire is 7.4 μm long, morphologically uniform, and slightly tapered. The 2D map of the intensity of the PL emission varies substantially along the nanowire, with a particularly bright spot close to the middle of the nanowire. In Figure 2b, we extract spectra collected at two different points along the nanowire (marked as sections AA′ and BB′ in Figure 2a), which show that the emission energy and lineshape are remarkably uniform at different positions along the nanowire. Moreover, the PL spectrum obtained by integrating the PL from the entire nanowire is very similar. Each of these PL spectra exhibit a broad (FWHM ~25 meV) peak at 1.518 eV, which corresponds to energy of excitonic emission in bulk GaAs epilayers, and a lower energy shoulder, which can be attributed to defect-related luminescence.

Semiconductor nanowires of thicknesses more than twice the exciton Bohr radius (the case here) do not exhibit quantum confinement effects, but the dielectric contrast between the nanowire and its surroundings results in significant polarization anisotropy.[17,18,20,21] This is true also for these GaAs−AlGaAs nanowires (ϵ = 12.5). We have previously observed that a significant increase in PL intensity (by a factor of ~70) occurs when the exciting laser is polarized along the nanowire versus perpendicular to it.[17]

In the present work, we have studied the polarization of the nanowire emission as a function of laser excitation energy. For most of the measurements discussed here, the laser was linearly polarized along the nanowire axis so that excitons were excited into well-defined excitonic spin states. The resultant PL images were obtained for polarized PL, analyzed both parallel and perpendicular to the nanowire. The resulting polarization-resolved 2D PL images of wire 2 are displayed in Figure 3a, the emission component polarized parallel to the wire, and Figure 3b, the perpendicularly polarized component. Note that the 2D images of wire 2 (~8 μm long) are quite similar to the PL image of wire 1 (Figure 2) and display the same broad emission band along the entire length of the nanowire, with PL intensity strongly peaked at one position along the nanowire. To determine the polarization of the emission, the two orthogonally polarized images (Figure 3a and b) are combined pixel by pixel and the polarization calculated as $P = (I_{\parallel} - I_{\perp})/(I_{\parallel} + I_{\perp})$. The result of this calculation is shown as the image in Figure 3c. The nanowire emission appears to be strongly polarized (~80%) along the nanowire throughout its length. A histogram of the polarization for a set of pixels defined by the spatial and spectral ranges outlined by the box in Figure 3c is displayed in Figure 3d. The average degree of polarization determined from this distribution is 82%, with a variation of approximately ± 3 %.

With these techniques, we can measure both the integrated intensity and the polarization of the PL emission from the GaAs/AlGaAs core−shell nanowires as the excitation laser is scanned from high energy down into resonance with the emission band. Recording the emission intensity as a function of excitation energy is equivalent to obtaining a standard photoluminescence excitation (PLE) spectrum. In Figure 4a and 4b, we show PL (solid lines) and PLE (symbols) spectra

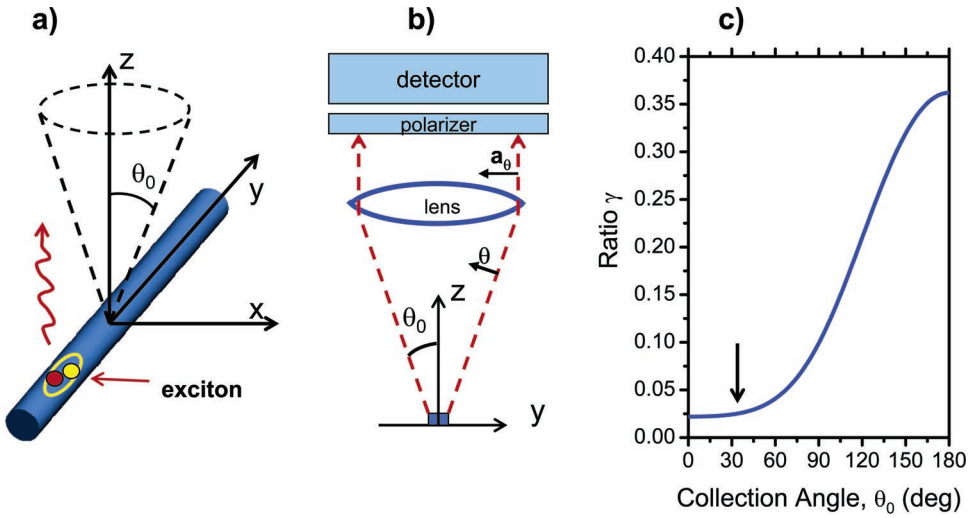

Figure 5. (a and b) Geometries of the system and experiment. (c) Calculated ratio of emission intensities (γ, eq 3) for an ideal wire in the limit of large relative energy; this limit corresponds to a randomized spin distribution of excitons.

for wires 1 and 2, respectively. Both nanowires exhibit a series of peaks in the PLE spectra where significant enhancement of the PL emission intensity from the nanowire occurs. The energies of the first two resonances, at ~36 meV and ~73 meV above the free exciton emission energy, occur at multiples of the LO phonon energy in bulk GaAs (36.5 meV). Therefore, we ascribe those resonances to the enhancement of PL intensity for excitation energies that allow rapid, resonant phonon relaxation down to the bottom of the band through the emission of 1 or 2 longitudinal optical (LO) phonons. The third resonance at ~135 meV can be tentatively assigned to the resonant excitation of the carriers in the AlGaAs shell, followed by capture and radiative recombination in the GaAs core. The energy of this resonance corresponds to an AlGaAs band gap with 10% Al composition. This is a significantly smaller Al composition than one would expect for epilayer growth under the same conditions.

A key result of this investigation is displayed in Figure 4c, where the polarization of the PL emission from nanowires 1 and 2 as a function of the excitation energy is presented. The incident laser, which is polarized parallel to the nanowire, excites exciton quantum states, with dipoles aligned parallel to the nanowire. If these excitons achieve thermal equilibrium, one should expect equal densities of excitons aligned along all three axes. For *equal populations* of excitons with dipoles aligned parallel and perpendicular to the nanowire, the PL is expected to be strongly polarized (92% for our case, $\epsilon = 12.5$), as has been calculated classically by several researchers.[18,20,21] At the highest excitation energies, we observe the emission polarizations from wires 1 and 2 to be *significantly smaller* than this value, and moreover, the polarizations are quite different from each other, 82% versus 75%. However, for both wires, the degree of polarization increases as the excitation energy comes closer to resonance with the PL emission band. Because the emission energy *does not change* as the excitation energy is scanned, we do not expect the classical degree of polarization for equal exciton distributions to change either. We therefore attribute the increasing emission polarization to a corresponding development of increasingly nonequilibrium exciton distributions.

These nonequilibrium polarized exciton distributions can also be seen for wire 2, where the excitons are excited into the nanowire with the laser polarized *perpendicular* to the nanowire. While much less efficient[17] (by a factor of 70) than the previous case, with much longer averaging times (10 min compared with 1 min), we can observe the emission polarization. We find that, at the lowest energies, the emission is *nevertheless polarized parallel* to the nanowire because even the small density of excitons parallel to the nanowire emit much more efficiently than those with dipoles aligned perpendicular to the nanowire. Remarkably, as the laser is tuned to higher energies, the emission polarization *increases.* At higher energies, the excitons scatter more, depolarizing the exciton distributions into the radiatively efficient exciton dipoles aligned parallel to the nanowire. The fact that at the highest energies the emission polarization is approximately the *same* for parallel and perpendicular pumping indicates that the densities of the excitons are approaching thermal equilibrium, or equal densities. The dynamics of exciton recombination as well as the spin-scattering times are intimately involved in understanding this data, as we will now discuss.

Because there is no quantum confinement in these 40 nm nanowires,[18,20,21] the exciton wavefunctions are spherically symmetric, and the optically active exciton state wavefunctions can be written as $|\mathbf{x}\rangle$, $|\mathbf{y}\rangle$, and $|\mathbf{z}\rangle$, where the index $\alpha = x,y,z$ specifies a dipole moment direction of a particular state. The direction y corresponds to the NW axis, and the lens collects photons propagating from the NW within the angle θ_0 around the z-axis (Figure 5a). Note that, while the light polarizer selects photons either with $\parallel$ or $\perp$ polarizations that correspond to the y and x directions in our system of coordinates (Figure 5a), the finite collection angle of the microscope objective (0.5 NA) means that each exciton state

(x,y,z) potentially contributes to the observed polarized luminescence. Thus, the intensity of light (photons/s) emitted from recombination of a population density of excitons of three types, n_α, is just determined by the probabilities $W_{\alpha\to\parallel}$ and $W_{\alpha\to\perp}$:

$$I_\perp = \sum_{\alpha=x,y,z} W_{\alpha\to\perp}\cdot n_\alpha, \qquad I_\parallel = \sum_{\alpha=x,y,z} W_{\alpha\to\parallel}\cdot n_\alpha \quad (1)$$

Because we observe $I_\parallel/I_\perp \gg 1$ and $\theta_0 = \pi/6 \ll \pi$ (the collecting system catches mostly photons with $k \parallel z$), we expect that $|\mathbf{y}\rangle$ excitons will dominate the PL signal. Simultaneously, the $|\mathbf{x}\rangle$ and $|\mathbf{z}\rangle$ exciton emissions are suppressed due to the dielectric properties of the NW.[18,20,21] The contribution of $|\mathbf{z}\rangle$ is suppressed further because of the small collection angle θ_0. We next provide a more quantitative discussion of these observations.

In the following, we consider a NW in a vacuum and ignore the effect of the silicon substrate. In addition, we will treat a single exciton as a two-level system. The radiative lifetimes of the excitons inside the NW can be calculated using the methods of quantum optics[22] and the approach used recently in ref 23. A quantum state of photons is given by two vectors ($\mathbf{k}$, $\mathbf{e}_\beta$), where the two polarization vectors $\mathbf{e}_\beta$ should be orthogonal to the photon wave vector, $\mathbf{k}$. The light−matter interaction is described by the operator $\hat{V}_{\text{int}} = -\hat{\mathbf{d}}\cdot\hat{\mathbf{E}}$, where $\hat{\mathbf{d}}$ and $\hat{\mathbf{E}}$ are the exciton dipole moment and photon electric field. Inside the nanowire, the electric field becomes partially screened: $\hat{E}_{x,z} = \hat{E}^0_{x,z}\, 2/(1+\epsilon_s)$ and $\hat{E}_y = \hat{E}^0_y$,[24] where $\hat{E}^0_\alpha$ are the field components in vacuum and ϵ_s is the relative dielectric constant of a semiconductor. The above equation is valid for a narrow wire, $r_{\text{NW}}/\lambda \ll 1$, where r_{NW} and λ are the NW radius and the wavelength of the emitted photons, respectively; this inequality is well satisfied in our experiments. Then, using Fermi's golden rule, we obtain the two different exciton lifetimes for dipoles oriented parallel (τ_y) and perpendicular (τ_x, τ_z) to the nanowire:

$$\tau_x = \tau_z = \tau_y\left(\frac{1+\epsilon_s}{2}\right)^2, \qquad \tau_y = \tau_{\text{vac}} = \frac{3\pi\epsilon_0\hbar c_0^{\,3}}{\omega_{\text{exc}}^3 d_{\text{exc}}^2} \quad (2)$$

where τ_{vac} is the lifetime of excited two-level system in vacuum,[22] d_{exc} and $\omega_{\text{exc}} = c_0 k$ are the interband dipole moment of the exciton and its frequency, respectively; ϵ_0 is the permittivity of vacuum. Because $\epsilon_s = 12.5$, $\tau_{x,z} \gg \tau_y$. We have seen above for wire 2, for instance, that the *emission* is strongly polarized *parallel* to the wire even while the *excitation laser* is polarized *perpendicular* to the wire directly. This result reflects this difference in radiative lifetimes for excitons oriented parallel and perpendicular to the wire, as reflected in eq 2.

To compute the probabilities $W_{\alpha\to\parallel}$ and $W_{\alpha\to\perp}$, we have to integrate over the vector $\mathbf{k}$ only within the cone $0 < \theta < \theta_0$ and also take into account the geometry of the experiment (see Figure 5b). Because the NW in our system can be treated as a point source, it is convenient to use spherical coordinates and introduce three unit orthogonal vectors (ρ, ϕ, θ). Then, one possible choice of emitted photon polarizations is $\mathbf{e}_\varphi = \phi$ and $\mathbf{e}_\theta = \theta$. Because of the cylindrical symmetry of the lens, the photons $\mathbf{e}_\varphi$ and $\mathbf{e}_\theta$ become transformed into photons with polarizations $\mathbf{a}_\varphi = -\sin\varphi\cdot\mathbf{x} + \cos\varphi\cdot\mathbf{y}$ and $\mathbf{a}_\theta = -\cos\varphi\cdot\mathbf{x} - \sin\varphi\cdot\mathbf{y}$, respectively. The polarizer selects either $\parallel$ ($\mathbf{y}$) photons or $\perp$ ($\mathbf{x}$) photons, and the corresponding photonic states can be represented as $\mathbf{e}_\perp = \mathbf{e}_x = \sin\varphi\cdot\mathbf{a}_\varphi + \cos\varphi\cdot\mathbf{a}_\theta$ and $\mathbf{e}_\parallel = \mathbf{e}_y = \cos\varphi\cdot\mathbf{a}_\varphi - \sin\varphi\cdot\mathbf{a}_\theta$, respectively. This result can be used to define new orthogonal photonic polarizations $\mathbf{b}_\perp = \phi\sin\varphi + \theta\cos\varphi$ and $\mathbf{b}_\parallel = \phi\cos\varphi - \theta\sin\varphi$. These photon polarizations have the convenient property that the lens provides the mapping $\mathbf{b}_\perp \to \mathbf{e}_x$ and $\mathbf{b}_\parallel \to \mathbf{e}_y$, where the photon states $\mathbf{b}_{\perp(\parallel)}$ are defined before entering the lens and $\mathbf{e}_{x(y)}$ are the photon states after passing the lens. For example, the $\mathbf{x}$-polarizer will transmit the photons $\mathbf{b}_\perp$ and completely block the photons $\mathbf{b}_\parallel$. The emission probabilities are then easily expressed as

$$W_{\alpha\to\perp} = \frac{2\pi d_{\text{exc}}^2(\hbar\omega_{\text{exc}})^2}{4\hbar\epsilon_0}\sum_{\mathbf{k},0<\theta<\theta_0} R_\alpha(\mathbf{b}_\perp\cdot\alpha)^2\,\delta(\hbar\omega_{\text{exc}} - \hbar c_0 k),$$
$$W_{\alpha\to\parallel} = \frac{2\pi d_{\text{exc}}^2(\hbar\omega_{\text{exc}})^2}{4\hbar\epsilon_0}\sum_{\mathbf{k},0<\theta<\theta_0} R_\alpha(\mathbf{b}_\parallel\cdot\alpha)^2\,\delta(\hbar\omega_{\text{exc}} - \hbar c_0 k) \quad (3)$$

where $R_{x(z)} = R = (2/(1+\epsilon_s))^2$and $R_y = 1$ are the screening factors. This factor appears only next to the $\mathbf{x}$- and $\mathbf{y}$-components of the polarization vectors $\mathbf{b}_{\perp(\parallel)}$. By integration over the collecting cone in $\mathbf{k}$-space, we derive the collection probabilities $W_{\alpha\to\perp(\parallel)}(\theta_0)$. This procedure can be seen in detail in the Supporting Information.

In our resonant excitation experiments, we have found that, as the energy of the laser (polarized $\parallel$ to the wire) moves closer and closer to resonance with the emission line, the degree of polarization strongly increases (see Figure 4c). As we will show, this occurs because the exciton populations must be out of equilibrium with $n_y > n_x = n_z$. At higher excitation energies, however, the excitons must rapidly thermalize through numerous scattering events, which may relax both momentum and spin. Thus, at higher excitation energies, the emitting exciton population must be close to thermal equilibrium with $n_x = n_y = n_z$. In this case, the intensity ratio,

$$\gamma(\theta_0) = \frac{I_\perp}{I_\parallel} = \frac{\sum_{\alpha=x,y,z} W_{\alpha\to\perp}}{\sum_{\alpha=x,y,z} W_{\alpha\to\parallel}}, \quad (4)$$

can be computed. $\gamma(\theta_0)$ strongly increases with the collection angle θ_0 (see Figure 5c). The reason is that, for small θ_0, only $\mathbf{x}$-excitons with $\mathbf{k} \parallel \mathbf{z}$ contribute to the signal $I_\perp$. Because

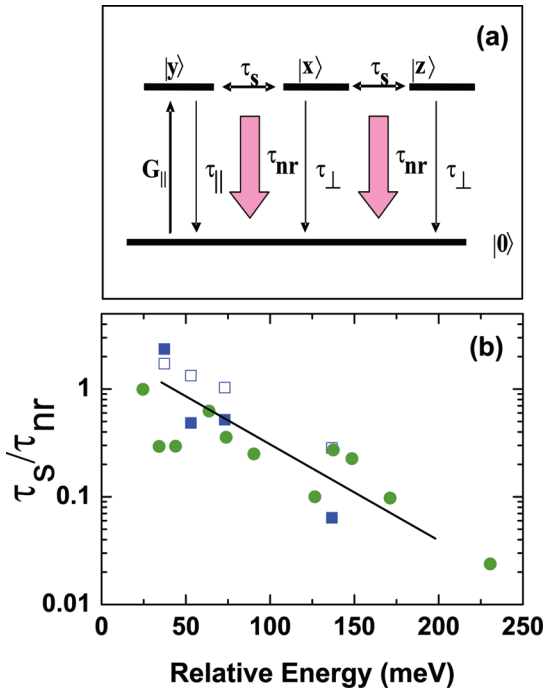

Figure 6. (a) Schematic diagram of exciton basis states and transitions between them; (b) ratio of spin scattering time to nonradiative lifetimes as a function of excitation energy for both wires and also for different pumping (wire 2). The symbol notations are identical to Figure 4c.

these excitons have reduced interaction with vacuum photons due to dielectric screening, their emission is suppressed; $\gamma(\theta_0 \rightarrow 0) = R \approx 0.022$. For large θ_0, the unscreened, bright **y**-excitons contribute to the signal $I_\perp$ and the ratio $\gamma(\theta_0)$ strongly grows. For our experimental geometry, $\gamma(\theta_0 = 30°) \approx 0.025$. Figure 4c shows the polarization, $P = (I_{||} - I_\perp)/(I_{||} + I_\perp)$, for both wires 1 and 2 as a function of the relative energy $\Delta\omega = \omega_{laser} - \omega_{exc}$. For high $\Delta\omega$, $P \rightarrow 0.88$ and 0.75 for wires 1 and 2, respectively. With the above numbers ($\gamma(\theta_0 = 30°) \approx 0.025$), our model gives $P = 0.95$. The discrepancy between experiment and theory might be attributed to NW defects and roughness; it is clear from Figure 4c that P is sample dependent.

To model these experiments further, we now consider optically created excitons, which can then recombine radiatively or nonradiatively or scatter between the states, as shown in Figure 6a. Because we have found that the recombination lifetime for excitons in the GaAs/AlGaAs nanowire is less than 80 ps, it is clear that the excitons are dominated by nonradiative recombination.[17] Moreover, because we observe a significant nonthermal population of spins, the spin-scattering rate must be comparable to the nonradiative lifetime. Thus we consider a hierarchy of relaxation times: $\tau_x = \tau_z \gg \tau_y \gg \tau_{nr}, \tau_s$ where τ_{nr} and τ_s are nonradiative and spin lifetimes, respectively. We consider the case where all times are constants, except the spin-scattering time which changes with the laser excitation energy. The coupled rate equations are thus:

$$\frac{dn_x}{dt} = G_\perp - \frac{n_x}{\tau_\perp} - \frac{n_x}{\tau_{nr}} - 2\frac{n_x}{\tau_s} + \frac{n_y}{\tau_s} + \frac{n_z}{\tau_s}$$

$$\frac{dn_y}{dt} = G_{||} - \frac{n_y}{\tau_{||}} - \frac{n_y}{\tau_{nr}} - 2\frac{n_y}{\tau_s} + \frac{n_x}{\tau_s} + \frac{n_z}{\tau_s}$$

$$\frac{dn_z}{dt} = -\frac{n_y}{\tau_\perp} - \frac{n_y}{\tau_{nr}} - 2\frac{n_y}{\tau_s} + \frac{n_x}{\tau_s} + \frac{n_z}{\tau_s}$$

where $\tau_\perp = \tau_{x(z)}$, $\tau_{||} = \tau_y$, and $G_\perp$ and $G_{||}$ are the pumping rates for the excitation beams with $\perp$ and || polarizations, respectively. We solve these coupled equations in steady state ($dn_\alpha/dt = 0$), neglecting the radiative recombination rate for all exciton populations.

In addition, we simplify the equations of eq 1: $I_\perp \approx W_{x\rightarrow\perp} \cdot n_x$, $I_{||} \approx W_{y\rightarrow||} \cdot n_y$. This simplification is valid for small collection angles ($\theta_0 \ll \pi$). Then, we obtain the result:

$$P = \frac{I_{||} - I_\perp}{I_{||} + I_\perp} = \frac{1 - \frac{n_x}{n_y}\gamma_1}{1 + \frac{n_x}{n_y}\gamma_1} = \frac{1 + \frac{\tau_s}{\tau_{nr}} - \gamma_1}{1 + \frac{\tau_s}{\tau_{nr}} + \gamma_1},$$

($G_\perp = 0$, $G_{||} \neq 0$) parallel pumping

$$P = \frac{\frac{1}{\gamma_1} - 1 - \frac{\tau_s}{\tau_{nr}}}{\frac{1}{\gamma_1} + 1 + \frac{\tau_s}{\tau_{nr}}},$$

($G_\perp \neq 0$, $G_{||} = 0$) perpendicular pumping (5)

where $\gamma_1 = W_{x\rightarrow\perp}/W_{y\rightarrow||}$. If we assume that the polarization at the highest energy for $G_{||} \neq 0$ occurs when $n_z = n_y = n_x$, this sets the ratio γ_1, which is equal to $^1/_{16}$ for wire 1 and $^1/_7$ for wire 2, which results in polarizations of 88% and 75%, respectively. As the excitation energy decreases, the data (see Figure 4) indicates that significantly nonequilibrium exciton distributions result. The rate equations (eq 5) show that the degree of nonequilibrium exciton distributions is substantial at the lowest excitation energies, with parallel excitation yielding $n_y/n_x = 2.4$ for wire 1 and 3.4 for wire 2, while for perpendicular excitation of wire 2, $n_x/n_y = 2.7$. This dramatic change in the exciton distributions for resonant excitation must result from a significant change in the exciton spin relaxation time.

Using eqs 5, we can estimate the changing spin relaxation rates through the ratio

$$\frac{\tau_s}{\tau_{nr}} = \gamma_1\left(\frac{1+P}{1-P}\right) - 1$$

for parallel pumping and

$$\frac{\tau_s}{\tau_{nr}} = \frac{1}{\gamma_1}\left(\frac{1-P}{1+P}\right) - 1$$

for perpendicular pumping. In this way, we can extract the ratio τ_s/τ_{nr} directly for all the data in Figure 4a. The results of this analysis are displayed in Figure 6b. Remarkably, all data for both wires and different excitation polarizations in Figure 6b group well on one line with a negative derivative. From this, we can say that the ratio τ_s/τ_{nr} ranges from 0.1 at the highest energies to 1 as the laser comes close to resonance.

As mentioned previoiusly, time-resolved PL measurements show that the nonradiative recombination lifetime is less than 80 ps (our system response). We believe that $\tau_{NR} = 50$ ps is a reasonable estimate of the nonradiative recombination lifetime, which reflects both the known upper bound determined by our system response and a lower bound suggested by the observed PL intensity when compared to other single nanostructures with longer recombination lifetimes. This places an upper bound to the spin lifetime ranging from 5 ps at high energies to greater than 50 ps at lower energies. The strongly nonequilibrium exciton distributions measured in these nanowires clearly result from the fact that the exciton recombination lifetime is limited by nonradiative recombination and so the excitons do not live long enough to randomize their spin profiles.

As noted by Planel and Benoit á la Guillaume in ref 25, linear polarization measurements (as discussed here) create well-defined exciton states that are linear combinations of the spherical $e-h$ wave functions. Neither the electron nor the hole are oriented by themselves; the linear polarization is a property of the $e-h$ pair. Because of this, any depolarization of either the electron or hole spin or their coherence will destroy the linear polarization of the pair.[25] For instance, in bulk GaAs, strong mixing of the light and heavy hole bands near $k = 0$ cause the hole spins to relax almost instantaneously ($\sim$100 fs),[26] and so linear polarization measurements are impossible in bulk GaAs unless the valence band degeneracy is lifted by uniaxial strain.[25] This suggests that here the light- and heavy-hole degeneracy may be lifted in these nanowires through strain, thereby increasing the hole spin lifetimes into the picosecond range.[25] Thus, the observed strong decrease in the scattering time at higher energies may result from valence band-mixing at energies larger than the light- and heavy-hole splitting, or increased electron−hole exchange.[25,27]

We also can make our model more complex by involving dark excitons. It is interesting that the results (eq 4) will hold even in the presence of dark excitons for the limit $\tau_\perp$, $\tau_{||} \gg \tau_{nr}, \tau_s$. Strictly speaking, the approach of the two-level system used in this paper is only valid for localized excitons with spherical symmetry. However, for the 3D free excitons confined inside the NW, the results in eqs 4 and 6 and displayed in Figure 5c remain valid. To account for the free exciton distribution, we should add the Boltzmann factor $e^{-\hbar^2 k_y^2(\theta,\varphi)/2m_{exc}k_BT}$ to the functions inside the sums in eqs 3. This approach assumes that the photon with $\mathbf{k} = (k_x,k_y,k_z)$ is created by the exciton with $\hbar\mathbf{k} = (0,\hbar k_y,0)$, i.e., only the **y**-component is conserved and $r_{NW}/\lambda \ll 1$. Because the photon wavelength is so long, the exponent is very small ($\hbar^2 k_y^2(\theta,\varphi)/2m_{exc}k_BT \leq 0.01$) and the Boltzmann factor does not make any difference. We assume here a typical temperature of 4 K and exciton mass of 0.5 m_0.

To summarize, we have studied the exciton spin and relaxation dynamics using polarization-sensitive spatially resolved PL imaging spectroscopy of single core−shell GaAs−AlGaAs NWs at low temperatures. Excitation data shows strong resonant enhancement of the broad PL emission line where the emission of 1- or 2-LO phonons enables rapid and efficient relaxation to the bottom of the exciton band. At the highest energies, where the excitons are close to thermal equilibrium, the emission PL is strongly polarized because the dielectric mismatch between the nanowire and the surrounding air results in strong suppression of the radiative recombination for excitons aligned perpendicular to the nanowire axis. Importantly, we have shown that the polarization of the PL emission is strongly enhanced as the laser comes closer to resonance with the exciton emission. This strong polarization enhancement is seen to result from the excitation of strongly nonequilibrium exciton distributions near resonance. Using rate equation modeling, we show that the spin relaxation time becomes comparable to the nonradiative recombination time when the exciton distributions are excited close to resonance. At higher energies, in contrast, the spin relaxation time decreases monotonically to $^1/_{10}$ the nonradiative recombination time.

Acknowledgment. This work was supported by the University of Cincinnati and by the Nano Biotechnology Initiative at Ohio University. The Australian authors gratefully acknowledge the financial support from the Australian Research Council.

Supporting Information Available: Derivation of the collection probabilities $W_{\alpha\to\perp(||)}(\theta_0)$. This material is available free of charge via the Internet at http://pubs.acs.org.

References

(1) Agarwal, R.; Barrelet, C. J.; Lieber, C. M. *Nano Lett.* **2005**, *5*, 917−920.
(2) Greytak, A. B.; Barrelet, C. J.; Li, Y.; Lieber, C. M. *Appl. Phys. Lett.* **2005**, *87*, 151103-1−151103-3.
(3) Gu, Y.; Kwak, E. S.; Lensch, J. L.; Allen, J. E.; Odom, T. W.; Lauhon, L. J. *Appl. Phys. Lett.* **2005**, *87*, 043111-1−151103-3.
(4) Gu, Y.; Romankiewicz, J. P.; David, J. K.; Lensch, J. L.; Lauhon, L. J. *Nano Lett.* **2006**, *6*, 948−952.
(5) Gudiksen, M. S.; Lauhon, L. J.; Wang, J.; Smith, D. C.; Lieber, C. M. *Nature* **2002**, *415*, 617−620.
(6) Sirbuly, D. J.; Law, M.; Pauzauskie, P.; Yan, H.; Maslov, A. V.; Knutsen, K.; Ning, C. Z.; Saykally, R. J.; Yang, P. *Proc. Natl. Acad. Sci. U.S.A.* **2005**, *102*, 7800−7805.
(7) Sirbuly, D. J.; Law, M.; Yan, H. Q.; Yang, P. D. *J. Phys. Chem. B* **2005**, *109*, 15190−15213.
(8) Barrelet, C. J.; Greytak, A. B.; Lieber, C. M. *Nano Lett.* **2004**, *4*, 1981−1985.
(9) Lauhon, L. J.; Gudiksen, M. S.; Lieber, C. M. *Philos. Trans. R. Soc. London, Ser. A* **2004**, *362*, 1247−1260.
(10) Lauhon, L. J.; Gudiksen, M. S.; Wang, C. L.; Lieber, C. M. *Nature* **2002**, *420*, 57−61.
(11) Samuelson, L.; Thelander, C.; Bjork, M. T.; Borgstrom, M.; Deppert, K.; Dick, K. A.; Hansen, A. E.; Martensson, T.; Panev, N.; Persson, A. I.; Seifert, W.; Skold, N.; Larsson, M. W.; Wallenberg, L. R. *Physica E* **2004**, *25*, 313−318.
(12) Borgstrom, M. T.; Zwiller, V.; Muller, E.; Imamoglu, A. *Nano Lett.* **2005**, *5*, 1439−1443.
(13) Fasth, C.; Fuhrer, A.; Bjork, M. T.; Samuelson, L. *Nano Lett.* **2005**, *5*, 1487−1490.

(14) Hewaparakrama, K. P.; Wilson, A.; Mackowski, S.; Jackson, H. E.; Smith, L. M.; Karczewski, G.; Kossut, J. *Appl. Phys. Lett.* **2004**, *85*, 5463−5465.
(15) Mackowski, S.; Gurung, T.; Jackson, H. E.; Smith, L. M.; Karczewski, G.; Kossut, J. *Appl. Phys. Lett.* **2005**, *87*, 72502-1−72502-3.
(16) Titova, L. V.; Hoang, T. B.; Jackson, H. E.; Smith, L. M.; Yarrison-Rice, J. M.; Lensch, J. L.; Lauhon, L. J. *Appl. Phys. Lett.* **2006**, *89*, 053119-1−053119-3.
(17) Titova, L. V.; Hoang, T. B.; Jackson, H. E.; Smith, L. M.; Yarrison-Rice, J. M.; Kim, Y.; Joyce, H. J.; Tan, H. H.; Jagadish, C. *Appl. Phys. Lett.* **2006**, *89*, 173126-1−173126-3.
(18) Wang, J. F.; Gudiksen, M. S.; Duan, X. F.; Cui, Y.; Lieber, C. M. *Science* **2001**, *293*, 1455−1457.
(19) Law, M.; Goldberger, J.; Yang, P. D. *Annu. Rev. Mater. Res.* **2004**, *34*, 83−122.
(20) Ruda, H. E.; Shik, A. *Phys. Rev. B: Condens. Matter* **2005**, *72*, 115308-1−115308-11.
(21) Ruda, H. E.; Shik, A. *J. Appl. Phys.* **2006**, *100*, 024314.
(22) Loudon, R., *Quantum Theory of Light*, 2nd ed.; Oxford University Press: New York, 1983.
(23) Govorov, A. O.; Bryant, G. W.; Zhang, W.; Skeini, T.; Lee, J.; Kotov, N. A.; Slocik, J. M.; Naik, R. R. *Nano Lett.* **2006**, *6*, 984−994.
(24) Jackson, J. D., *Classical Electrodynamics*, 2nd ed.; Wiley: New York, 1975.
(25) Meier, F.; Zakharchenya, B., *Optical Orientation*; North Holland: Amsterdam, 1984.
(26) Oudar, J. L.; Migus, A.; Hulin, D.; Grillon, G.; Etchepare, J.; Antonetti, A. *Phys. Rev. Lett.* **1984**, *53*, 384−387.
(27) Baylac, B.; Arnand, T.; Marie, X.; Dareys, B.; Brousseau, M.; Bacquet, G.; Thierry-Mieg, V. *Solid State Commun.* **1995**, *93*, 57−60.

NL062383Q